Energy 253 (2022) 124083

Contents lists available at ScienceDirect

Energy

journal homepage: www.elsevier.com/locate/energy

Design and characterization of a novel finned tubular thermoelectric generator for waste heat recovery

Mohamed Amine Zoui [a, b], Said Bentouba [a, c], Dhayalan Velauthapillai [c], Nadjet Zioui [d], Mahmoud Bourouis [e, *]

[a] Laboratory of Sustainable Development and Computing (LDDI), University of Adrar, 01000, Adrar, Algeria
[b] Laboratory of Energy, Environment, and Information Systems (LEESI), University of Adrar, 01000, Adrar, Algeria
[c] Western Norway University of Applied Sciences, Faculty of Engineering and Science, Bergen, 5063, Norway
[d] Mechanical Engineering Department, University of Quebec at Trois-Rivieres, QC, Canada
[e] Department of Mechanical Engineering, Universitat Rovira i Virgili, Av. Països Catalans No. 26, 43007, Tarragona, Spain

ARTICLE INFO

Article history:
Received 7 November 2021
Received in revised form
19 April 2022
Accepted 20 April 2022
Available online 27 April 2022

Keywords:
Tubular thermoelectric generator
Finned tube
Waste heat recovery
ANSYS-Fluent
Quadratic-profiled legs
Thermoelectric segment

ABSTRACT

Most commercial thermoelectric modules have a flat design that complicates their integration into gas/liquid thermoelectric conversion systems. The aim of the present study is to develop a robust, compact, and cost-effective design that is easier to incorporate into gas/liquid thermoelectric energy recovery systems. The description entails a novel finned tubular thermoelectric generator (FTTEG) prototype with three distinguishing characteristics: (i) quadratic-profiled thermoelectric legs arranged axially, (ii) a resin-based semi-rigid assembly, and (iii) annular heat exchange fins.

Module properties such as contact resistance, resin properties and heat exchanger performance were investigated using a numerical model developed with ANSYS-Fluent. Exchanger thermal efficiency was thus found maximal at a fin spacing of 2–3 mm and a fin height of 11–13 mm at the conditions of operation defined.

A test bench was built to evaluate the ability of the module to generate electrical power from hot water against forced ambient air. An output power of 16 mW at 600 mV open-circuit voltage was generated during tests with a temperature gradient of 60 °C.

1. Introduction

Pollution of the atmosphere is now recognized as an existential threat to human life on a global scale. To slow down the resulting climate change, many countries are required to limit their greenhouse gas emissions. This can be achieved by reducing the consumption of fossil fuels, by means of energy conservation and development of renewable energy. The recycling of waste energy is emerging as a promising solution, especially for industries that use large amounts of energy for production processes which release much of it into the environment as heat transported generally by air or water.

Thermoelectric materials have the property of converting heat flow into electrical energy via the Seebeck effect and vice versa via the Peltier effect [1]. They represent promising alternatives as future energy sources, especially when recycling the heat wasted during energy conversion to electricity, which increases system efficiency and reduces environmental pollution. Discovered two centuries ago, these materials have yet to be utilized in any practical energy recovery technology, due to their low conversion efficiency when compared to other waste heat recovery systems such as the organic Rankine cycle (ORC). However, their advantage consists in the direct conversion of energy, no moving parts (no vibration), limited maintenance and easier installation. Two main lines of research could bring about an advance towards this goal, namely (i) creating and developing more efficient thermoelectric materials, and (ii) creating more efficient thermoelectric generator designs which can be better integrated into overall energy conversion processes.

Conventional commercial TEG modules are essentially flat structures composed of 10–100 thermoelectric elements or “legs” connected electrically in series by conductive tabs and thermally connected in parallel and mounted between two ceramic layers. Two types of elements, n and p, alternate in each series. When a

* Corresponding author.
E-mail address: mahmoud.bourouis@urv.cat (M. Bourouis).

https://doi.org/10.1016/j.energy.2022.124083

Nomenclature

α	Seebeck coefficient, $\mu V \cdot K^{-1}$
σ	Electrical conductivity, $Ohm^{-1}\ cm^{-1}$
κ	Thermal conductivity, $W \cdot m^{-1}\ K^{-1}$
T	Temperature, K
C	Specific heat capacity, $J \cdot kg^{-1}\ K^{-1}$
R_L	Load resistance, Ohm
V_{OC}	Open circuit voltage, mV
V_L	Load resistance voltage, mV
R_m	Module internal resistance, Ohm

temperature gradient occurs between the ceramic faces, an electrical current is generated by the flow of electrons in the n-type legs and holes in the p-type legs. This is called the Seebeck effect. Heat is thus converted into electricity. The module designs can be cylindrical, thin or thick film and flexible [2].

A thermoelectric generating system thus operates in a dithermal medium, that is, hot and cold, by creating heat flow through the elements to generate an electric current. This thermal circuit consists of three essential components:

- Heat and cold sources transported by liquid or gas.
- A thermoelectric generator.
- A system of directing heat flow through the module (a heat sink in most cases).

The third component is the link between the first two and is characterized by its thermal resistance and heat transfer capacity. The lower the resistance and the higher the capacity and the better is the overall performance of the system.

Heat is transported to or from the module by a liquid or gas. The engineering of such a system therefore requires techno economic optimization through simple and coherent harmonization of its different components. For instance, flat modules are ideal for applications where the heat flow is perpendicular to the module faces. However, most industrial manufacturing waste heat flow is through cylindrical pipes, the heat source often being 1 cm in diameter. This makes it extremely challenging and the heat very costly to recover with rigid flat modules. A tubular module configuration would be much more practical in this situation.

Tubular TEGs are technically difficult to construct and have received little attention from scientific investigators. Min and Rowe [3] have described a module composed of four ring-shaped thermoelements built using the spark-erosion technique. The alternating n-type and p-type thermoelectric materials are arranged coaxially in the form of flat annular washers, with copper rings on the inner and outer edges to provide electrical connectivity in series. The gaps between them are filled with electrical and thermal insulators. Electrical bonding is achieved using solder paste heated to 200 °C. The performance of this prototype fell short of theoretical performance values because of the contact resistance between the thermoelectric rings and because the heat flow was perpendicular to the preferable direction of crystal growth. This suggests that crystal growth may be a poor choice for manufacturing ring-shaped thermoelectric elements.

Schmitz et al. [4] used the powder method (spark plasma sintering) instead of the crystal growth method to obtain ring-shaped TEG modules made of lead tellurium. The conductors were cylindrical and bonded directly to the inner and outer edges of the rings, which were respectively 9.3 mm and 14.3 mm in diameter and 1 mm thick.

Takahashi et al. [5] used spark plasma sintering in thermoelectric material and metal to obtain tilted layers of bismuth and nickel telluride on a tubular module with outer and inner diameters of 14 mm and 10 mm. This transverse thermoelectric device generated up to 2.7 W at a temperature differential of 85 °C. The authors claim that this design offers a high-power density (10 kW m^{-3}) compared to that of conventional annular TEG designs, despite its low efficiency (0.2%) due to the low ZT value (0.144) using nickel as for n-type elements.

The tubular module of Sakai et al. [6] allows for both power generation and Peltier cooling. The module was obtained by stacking the annular components axially, followed by simultaneous sintering and assembly. Power densities of up to 0.9 kW m^{-3} and 2.2% conversion efficiency were obtained experimentally at a ΔT of 85 K. Peltier effect refrigeration reached a ΔT of 49 K and a power density of 32.6 kW m^{-3}. However, these results were obtained at low temperatures because bonding with the low melting temperature abrasive is impossible at high temperatures. Such a module must be designed carefully to tolerate the mechanical stresses between the components which occur at high temperature gradients. Jang et al. [7] has shown that modified resistance welding performed by spark plasma sintering provides adequate bonding for manufacturing tubular modules for operation at higher temperatures and it is scalable.

In the studies mentioned above, different methods were used to make similar ring-shaped thermoelements. Theoretical studies are broader in scope, focusing on the performance of tubular or annular modules of a specific geometrical configuration. Shen et al. [8] predict the one-dimensional steady-state heat conduction of an annular model consisting of paired angular p and n legs arranged around a cylindrical heat source with a concentric heat sink at a constant temperature. Zhang et al. [9], exploring the effect of thermoelement geometrical configurations on annular thermoelectric generator performance, found that the power output per unit mass of an ideal generator is maximal only when the thermoelectric leg cross section is constant. Shen et al. [10] propose a segmented annular thermoelectric generator, a two-segment version of which has been analyzed for performance and stress [11,12]. Segmented generators appear to offer greater possibilities for improving power output and conversion efficiency compared to non-segmented generators [13].

Quadratic-profiled elements used in flat modules could be a suitable alternative to ring-shaped elements in order to avoid production complexities and high manufacturing costs caused by mechanical imperfections. The optimized geometry of this type of element provides high efficiency, better thermomechanical stability and can be reproduced in large-scale manufacturing.

The aim of the present study is to develop a robust, compact, and cost-effective tubular thermoelectric generator design that can be easily integrated into gas/liquid thermoelectric conversion systems. The module has the following distinctive characteristics: (i) quadratic-profiled and axially arranged thermoelectric legs, (ii) semi-rigid assembly with resin, (iii) incorporated annular heat-sink fins.

The thermal behaviour of the finned heat exchanger was simulated in silico to determine optimal dimensions such as fin height and fin spacing for the module design. The constructed module was evaluated on a test bench built especially for this purpose. The results of several tests are presented and discussed. The effects of physical parameters such as thermal and electrical contact resistance, air velocity, resin thermal conductance and resin layer thickness on module performance are also evaluated.

2. Module configuration, design, and fabrication

The finned tubular thermoelectric generator was designed to produce electrical energy by recovering waste heat from industrial processes and converting it directly into electricity. When hot fluid flows through the inner tube and cooling air flows around the fins or vice versa, the resulting temperature differential allows the module to generate electrical energy. The size of the assembled prototype is shown in Fig. 1I.

The outer tube, which supports the module assembly, is made of a copper alloy with good mechanical strength and thermal conductivity. Its wall thickness is 0.5 mm. The thermoelectric apparatus is made of alternating n-type and p-type Bi_2Te_3 legs arranged into segments as shown in Fig. 1D. The legs are very fragile and great care must be taken when assembling the segments and fixing them to the inside of the copper alloy tube. The segments are consolidated on aluminum strips 2.5 mm wide and 0.5 mm thick, using an electrically insulating and thermally conductive epoxy resin, as shown in Fig. 1F. Each segment is fixed to the inner surface of the copper tube using an adhesive varnish as shown in Fig. 1G. All legs and segments are connected electrically in series (Fig. 1H). The second role of the aluminum strip is to form the inner tube, which is coated with the same varnish to strengthen and waterproof it as illustrated in Fig. 2.

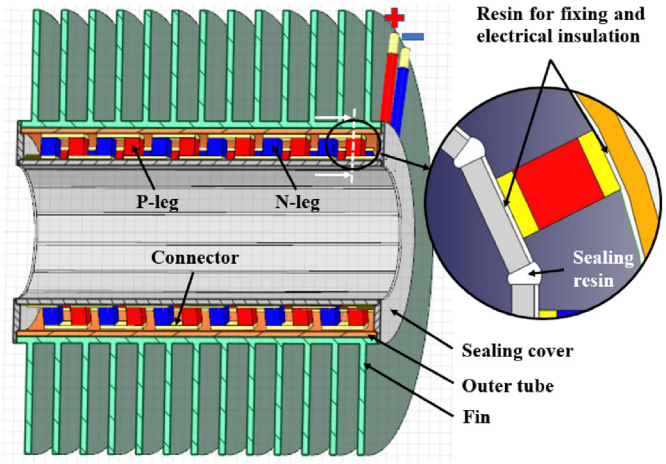

Fig. 2. 3D graphical illustration of the finned tubular thermoelectric generator design and position of the thermoelectric leg segments.

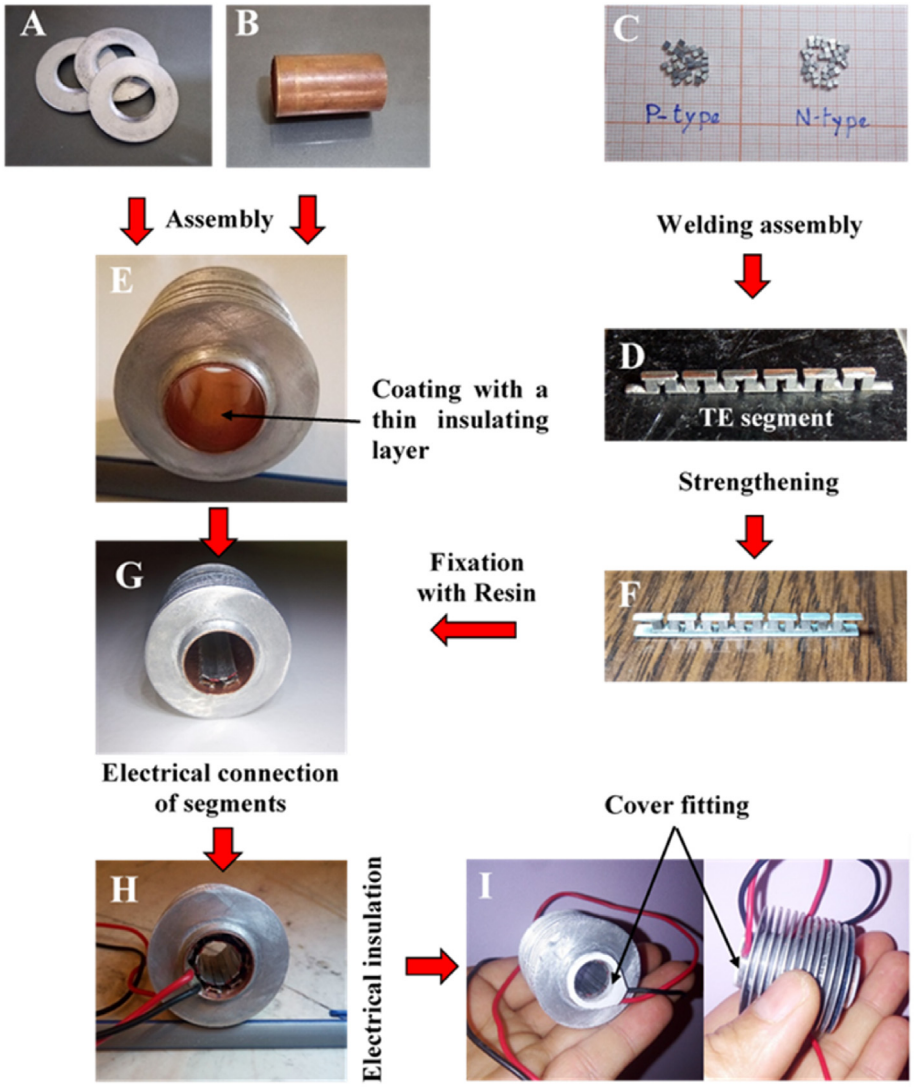

Fig. 1. Construction of the novel thermoelectric converter module.

The module thus contains 14 segments of 6 n-p pairs each for a total of 84 n-p pairs.

The aluminum annular fins slide snugly into the copper tube and remain in tight contact with each other by means of their flared inner edge (see Fig. 1A and E). The purpose of the fin assembly is to increase the surface area for heat exchange. However, this increased surface area also increases the pressure drop of any fluid flowing through the heat exchanger. This compromise must be balanced and must also consider fin material and manufacturing costs. Finned tube heat exchanger designs must therefore be optimized by maximizing heat transfer between the two media without creating an unacceptable pressure drop. The performance of the assembly as a heat sink can be simulated using ANSYS-Fluent. This can become quite complex if all parameters that influence heat transfer are taken into consideration. The authors suggest limiting this evaluation to the most influential parameters, namely fin height and fin pitch, and setting the remaining parameters as constants.

2.1. Fabrication of the thermoelectric segments

The basic functional element of the tubular thermoelectric converter is the segment of alternating n-type and p-type elements connected in electrical series as shown in Fig. 1D. The cross-sectional area of the tube may be circular, oval, oval-flat or polygonal, regardless of tube length or diameter. In the case of the present study, a circular cross-section has been used (Fig. 1B).

A special welding apparatus was created to obtain very straight thermoelectric segments with high-quality connections and high dimensional precision. The Bi_2Ti_3 coated Ti elements are rectangular prisms, 1.4 mm × 1.4 mm 1.64 mm as illustrated in Fig. 1C. The connectors are made of copper, 4 mm × 1.5 mm x 0.5 mm, the same as those used in flat modules. A low-melting (138 °C) Sn_{42} Bi_{58} solder paste was used [14]. The pressure applied during welding needs to be optimized since excess pressure can cause the leg to crack.

2.2. Simulation and construction of the heat sink

The function of the heat-sink portion of the tubular thermoelectric converter is to allow heat to dissipate from the module and thereby maintain a temperature differential between the two sides of the active elements. Heat is thus dissipated from the fins into the surrounding air. The fins also provide the module with mechanical strength. They were made by flaring aluminum washers slightly on the hole edge using a press built especially for this purpose. The tolerance of the flared portion is such that the fins can be stacked firmly with pressure so that they stay in contact with each other and form a single assembly on the outer tube as illustrated in Fig. 3.

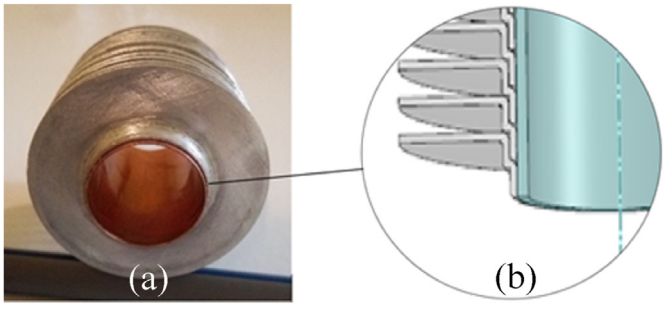

Fig. 3. (a) Photo of the finned tube; (b) A cross-section of the tube showing how the flared fin holes overlap.

Fluid flow and fin geometry have a major impact on the heat transfer and pressure drop across the device. Heat sink dimensions that gave optimal thermal and hydraulic performance for the intended conditions of operation were derived from an ANSYS-Fluent simulation based on several studies of heat exchanger tubes with annular fins [15–19]. The case of a single row of cross-flow finned tubes was used with the geometric and operational parameters set as follows: fin height (5–13 mm incremented 2 mm), fin spacing (1–4 mm incremented 1 mm), tube diameter 19 mm, and an ambient air velocity of 3 m s^{-1} at 30 °C in the test bench. Air flow is assumed to be three dimensional, incompressible, steady-state, and turbulent. A constant wall temperature of 90 °C is assumed in the tube. The results obtained using the RNG k–ε turbulence model of ANSYS-Fluent 19.2 show that heat transfer enhancement is concomitant with an increase in the pressure drop over the heat sink and heat transfer decreases as the pressure drop decreases. The overall efficiency gained using forced convection to minimize the influence of pressure drop must be weighed against the power consumed by the ventilation system. This makes the optimal geometry critical, since the choice of parameter will strongly influence the overall efficiency of the system.

Fig. 4 shows that spacing of 2–3 mm and a height of 11–13 mm are the ranges for optimal efficiency of the heat exchanger under the defined conditions of operation. Outside these ranges, either the pressure drop increases significantly or the total heat transfer rate decreases. Based on the simulation, a fin spacing of 2 mm and a fin height of 11 mm were considered appropriate for the present study.

3. Module characterization methodology

The thermal and electrical properties of the thermoelectric converter design were analyzed numerically. The electrical output of the prototype was measured on a test bench. Uncertain inputs in the simulations such as thermal and electrical contact resistance were calibrated using experimental results.

3.1. Experimental procedure

The test bench was set to provide a constant flow of air over the fins at 3 m s^{-1} and 30 °C as in the simulation, and a water flow rate of 20 L min^{-1} at a constant temperature stepped from 35 °C to 90 °C, at increments of 5 °C. The maximal power output of the thermoelectric module was determined when its resistance matched the resistance of the load. In practice, this power is measured easily when a temperature differential exists. To account for power fluctuations due to the Peltier effect, a circuit composed

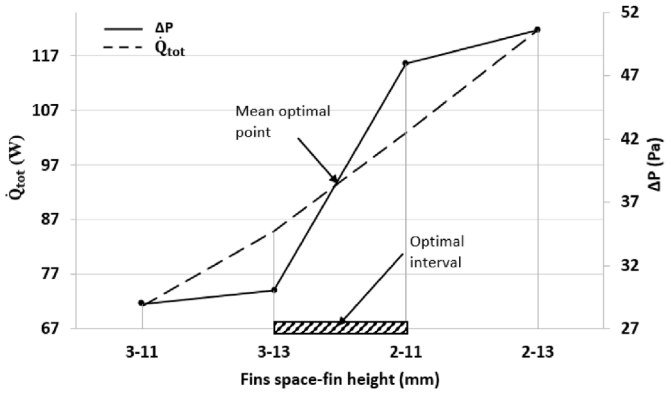

Fig. 4. The optimal ranges of heat sink fin spacing and height.

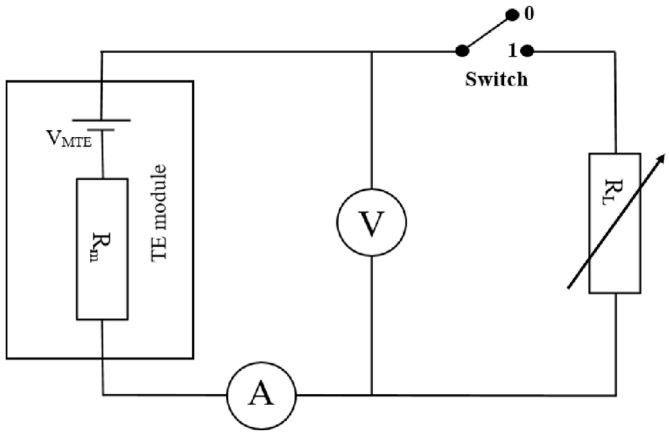

Fig. 5. Diagram of the test bench circuit with a loop selection switch.

of two loops (Fig. 5) and a switch were connected to the module to allow for measurement of the open circuit voltage (V_{OC}), the voltage (V_L), and the current (I) under load resistance. All measurements were taken when steady state conditions were achieved, and the load resistance ranged from 2 Ω to 22 Ω.

The maximal power output of the thermoelectric generator is calculated using equation (1):

$$P_{max} = \frac{V_{OC}^2}{4R_L(\frac{V_{OC}}{V_L} - 1)} \quad (1)$$

where R_L is the load resistance, V_{OC} is the open circuit voltage and V_L is the load resistance voltage. The electrical resistance of the module (R_m) can be calculated using equation (2):

$$R_m = R_L(\frac{V_{OC}}{V_L} - 1) \quad (2)$$

3.2. Computational procedure

The physical properties of the bismuth telluride (Bi_2Te_3) material, with which the thermoelectric legs are made, are temperature dependent. These include the Seebeck coefficient, thermal conductivity, and electrical resistivity. For the simulation, data provided by the manufacturer (Interm Thermoelectric Company) were used. The properties of the materials used to make the finned tubular thermoelectric generator are listed below (see Table 1).

The numerical simulation is performed using a two-way system coupling of the fluid flow CFX (fluid domain) with the thermal-electric (solid domain) on the ANSYS Workbench 19.2 platform. The software takes into account all relevant thermoelectric effects, namely Joule, Thomson, Peltier, and Seebeck [20]. The multi-physics fluid-thermoelectric model is based on the following assumptions: (i) steady state; (ii) incompressible air flow around the fins; (iii) gravity, radiative heat transfer and natural convection heat transfer are omitted, and (iv) thermal and electrical contact resistances are taken into consideration.

To save computational time, the model is simplified to 1/12 of its geometry as shown in Fig. 6a, to simulate only seven pairs of thermoelectric elements and two half-fins on the symmetrical cross-sectional and longitudinal planes. The grid system sizing selected to ensure grid independency is 0.3 mm hexahedral mesh for the solid domain (Fig. 6b), and 0.2 mm tetrahedral mesh for the fluid domain in regions where accuracy is reduced, such as around the tube wall and fins. In the remaining fluid regions, a 0.4 mm hexahedral mesh is sufficient. In addition, a five-layer boundary grid is applied to the contact surfaces between the solid and fluid regions to enhance coupling system simulation accuracy. The dimensions of the actual thermoelectric generator components made are the same as those used in the simulation and are listed in Table 2.

The critical challenge in manufacturing a thermoelectric generator is to maximize efficiency and ensure physically resistant and heat-stable contact between the parts. Both thermal resistance and electrical resistance associated with interfaces between materials should be taken into account when simulating module performance [21]. These resistances can have a significant effect and must be characterized.

Seven interfacial resistances are considered for two thermoelectric elements, as illustrated in Fig. 7. Five of these constitute a thermal resistance only ($R_{TC}1$, $R_{TC}2$, $R_{TC}3$, $R_{TC}6$, $R_{TC}7$) and two constitute both thermal and electrical resistances ($R_{TC}4$, $R_{TC}5$, $R_{EC}1$, $R_{EC}2$). The task is to define an average and reasonable value for each resistance in order to calibrate simulation input parameters for the prototype. This approach requires that all data reported in the literature be used to establish valid ranges. The goal is to predict numerically the thermal and electrical behaviour patterns of the prototype without costly additional experiments, and thus to improve performance by implementing design improvements that

Table 1
Physical properties of thermoelectric generator components.

Component	Material	Density ($kg\ m^{-3}$)	Specific heat capacity ($J\ kg^{-1}\ K^{-1}$)	Thermal conductivity ($W\ m^{-1}\ K^{-1}$)	Electrical conductivity ($Ohm^{-1}\ cm^{-1}$)	Seebeck coefficient ($\mu V\ K^{-1}$)
Leg, n or p type	Bi_2Te_3	7740	200	κ	σ	α
Connectors	Copper	8933	385	401	$56 \cdot 10^4$	–
Outer tube	Copper	8933	385	401	–	–
Fins, inner tube	Aluminum	2702	903	237	–	–
Insulating layer	Varnish	–	–	0.25	–	–

κ, σ or $\alpha = a_0 + a_1 \cdot T + a_2 \cdot T^2 + a_3 \cdot T^3 + a_4 \cdot T^4 + a_5 \cdot T^5 + a_6 \cdot T^6$ (T is absolute temperature)

	κ		σ		α	
	p type	n type	p type	n type	p type	n type
a_0	1.47	1.565	1145.23	1199	195.61	195.65
a_1	$2.17167 \cdot 10^{-3}$	$3.3984 \cdot 10^{-3}$	−7.5630	−5.35638	0.52104	0.31627
a_2	$2.26128 \cdot 10^{-5}$	$1.73219 \cdot 10^{-5}$	$3.4690 \cdot 10^{-2}$	$2.06045 \cdot 10^{-2}$	$-2.2343 \cdot 10^{-3}$	$-1.1739 \cdot 10^{-3}$
a_3	$3.23864 \cdot 10^{-8}$	$1.62686 \cdot 10^{-7}$	$-1.6825 \cdot 10^{-4}$	$9.2983 \cdot 10^{-5}$	$-5.8110 \cdot 10^{-6}$	$6.8552 \cdot 10^{-7}$
a_4	0	$1.8700 \cdot 10^{-9}$	$1.0245 \cdot 10^{-6}$	$3.4232 \cdot 10^{-9}$	0	0
a_5	0	$5.59604 \cdot 10^{-12}$	0	$1.5318 \cdot 10^{-9}$	0	0
a_6	0	0	0	$2.49716 \cdot 10^{-11}$	0	0

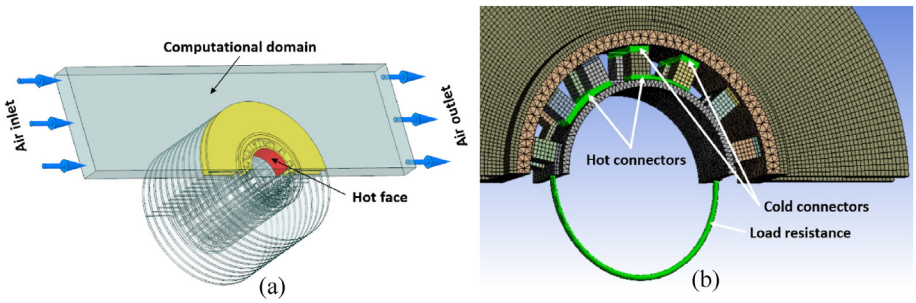

Fig. 6. (a) Thermoelectric generator simulation computational domain and boundary conditions; (b) Solid domain meshing.

Table 2
Dimensions of the finned tubular thermoelectric generator parts.

Parameter (mm)	n-type leg	p-type leg	Connectors	Outer tube	Inner tube	Finned tube
Section (length x width)	1.4 × 1.4	1.4 × 1.4	4 × 1.4	–	–	–
Outer diameter	–	–	–	19	13	42
Inner diameter	–	–	–	18	12	20
Thickness	1.64	1.64	0.4	1	0.5	0.6
Fin space	–	–	–	–	–	2

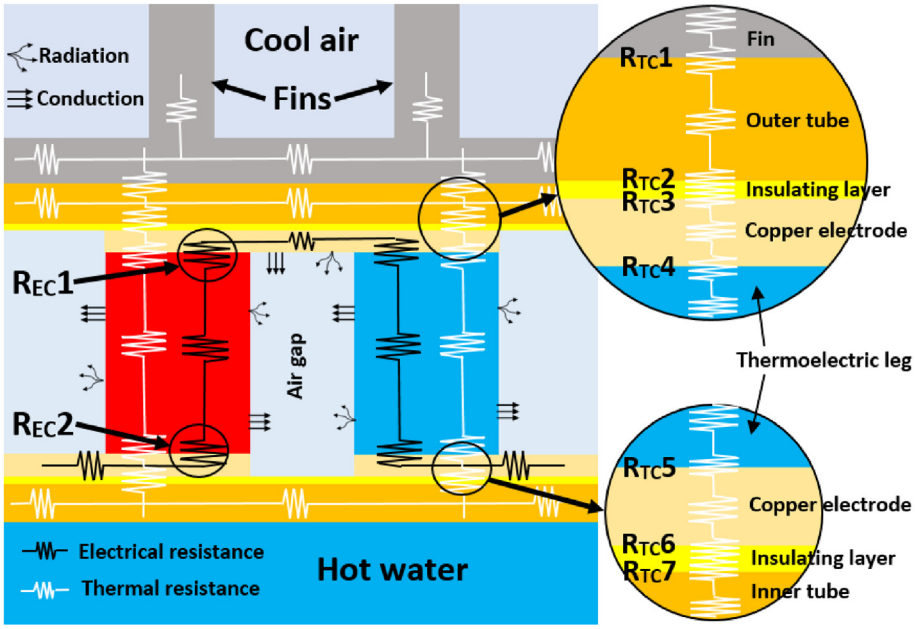

Fig. 7. Thermal and electrical contact resistance of a single p and n leg pair.

reduce contact resistances. Table 3 shows the values of contact resistances assumed in the prototype.

$R_{TC}1$ represents the thermal contact resistance between the fins and the outer tube. It is assumed to be in the range of 10–17 × 10^{-5} m^2 K W^{-1} [22–24].

$R_{TC}2$, $R_{TC}3$, $R_{TC}6$, $R_{TC}7$ represent the thermal contact resistances between copper and the insulating layer (varnish). Data on the thermal contact behaviour of adhesive polymers are scarce in the open literature. Thermal resistances are assumed to be in the range 25–67 × 10^{-5} m^2 K W^{-1}, based on three studies that are well in agreement [25–27].

The electrical contact resistances $R_{EC}1$ and $R_{EC}2$ are assumed to be equal and can be evaluated numerically with relative ease. They are reportedly in the range of 3–100 × 10^{-9} Ω m^2, depending on the manufacturing quality [29]. The corresponding thermal contact resistances $R_{TC}4$ and $R_{TC}5$ were set at 2 × 10^{-5} m^2 K W^{-1} [28].

The insulating layer was replaced with an overall thermal contact resistance calculated as follows:

$$R_{total} = R_{layer} + R_{contact\ a} + R_{contact\ b} \quad (3)$$

$$R_{layer} = \frac{d}{k} \quad (4)$$

where d and k are respectively the layer thickness and layer thermal conductivity, and $R_{contact\ a}$, $R_{contact\ b}$ represent the two interfaces of the layer.

Table 3
Thermal and electrical contact resistances used in the simulation.

Interface	Thermal contact resistance (m^2 K W^{-1})	Electrical contact resistance (Ω m^2)	Reference
$R_{TC}1$	10×10^{-5}	–	[22–24]
$R_{TC}2$, $R_{TC}3$, $R_{TC}6$, $R_{TC}7$	25×10^{-5}	–	[25–27]
$R_{TC}4$, $R_{TC}5$	2×10^{-5}	–	[28]
$R_{EC}1$, $R_{EC}2$	–	20×10^{-9}	–

4. Results and discussion

The novel prototype tubular heat-to-electricity converter module designed in this study consists of 14 axially arranged thermoelectric segments, each comprising 6 pairs of n-type and p-type bismuth telluride quadratically profiled legs connected in electrical series, for a total of 84 p-n pairs. The module was modeled numerically on the ANSYS Workbench 19.2 platform as a two-way system coupling fluid flow (CFX) and thermal-electric after being built and tested experimentally.

The generation of voltage (V) and current (I) by the module depends on a temperature differential existing between the inner pipe and the surrounding fin assembly. This difference will be maintained by hot water flowing in the pipe and relatively cool air flowing over the fins. The relationship between current and voltage for operation at any constant temperature is approximately linear (Fig. 8) if the internal resistance varies little over the temperature range. The increase in the open circuit voltage (V_{OC}) generated as ΔT increases is also linear (Fig. 9a). The measured voltage reaches 600 mV at ΔT = 60 °C (blue columns), which is maintained when hot water flows at 20 L min^{-1} and the ambient air is blown over the fins at 3 m s^{-1}. The red columns represent the results of the simulation based on the same input values as in the experiment and taking into consideration the assumed thermal contact resistances of Table 3. The deviation between the experimental and numerical open circuit voltages increases with temperature. This is due to parameters that were neglected in the simulation and are clearly temperature-dependent, namely conductive, and radiative thermal losses in different zones of the module as illustrated in Fig. 7. These losses increase with temperature increases and reduce the efficiency of the module. In addition, the thermal conductivity and the contact resistance of the insulating layer can largely increase the overall thermal resistance of the module. The deviation between the experimental and simulated V_{OC} output reached 22%.

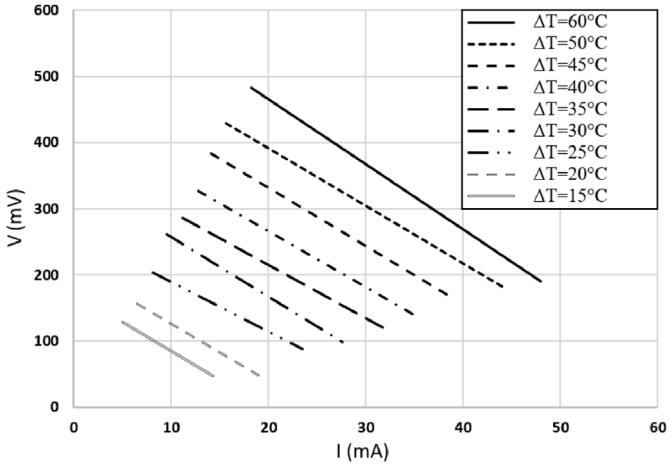

Fig. 8. Experimental results for voltage and current sweep at various temperature differentials.

These heat losses also have an impact on the maximal output power, as shown in Fig. 9b, which shows the same trend as in Fig. 9a. The blue and red columns again represent respectively experimental and computational results. Under the condition of equal load resistance R_L = 5.5 Ω, the resulting electrical contact resistance is 2×10^{-8} Ω m^2, and is in agreement with data reported elsewhere for the same leg dimensions and material [28].

The use of resin to join the inner and outer tubes makes the module less rigid and more able to absorb internal stresses resulting from the thermal expansion of different parts. With resin the module is less likely to crack. One study shows that the thermal conductance of some adhesives does not change significantly with variations in temperature and apparent pressure [27]. However, due to its very low thermal conductivity, the thin layer of resin has a significant influence on generator performance (Fig. 10a). The simulation shows that output power can be doubled by increasing the thermal conductivity of the resin from 0.25 to 2.4 W m^{-1} K^{-1}. Composite resins appear to have conductivities as high as 4.3 W m^{-1} K^{-1} [30,31]. The choice of a resin requires testing for elasticity, thermal conductivity, and layer thickness.

Fig. 10b shows that up to a certain point, increases in air velocity increase the thermoelectric conversion efficiency of the module. This is calculated as the actual output power relative to the output

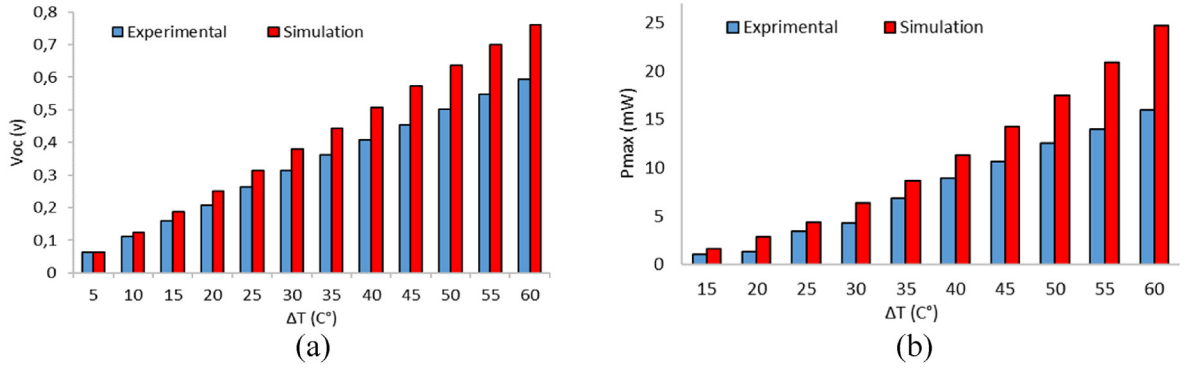

Fig. 9. Experimental versus simulation results: (a) Open circuit voltage, (b) Power max.

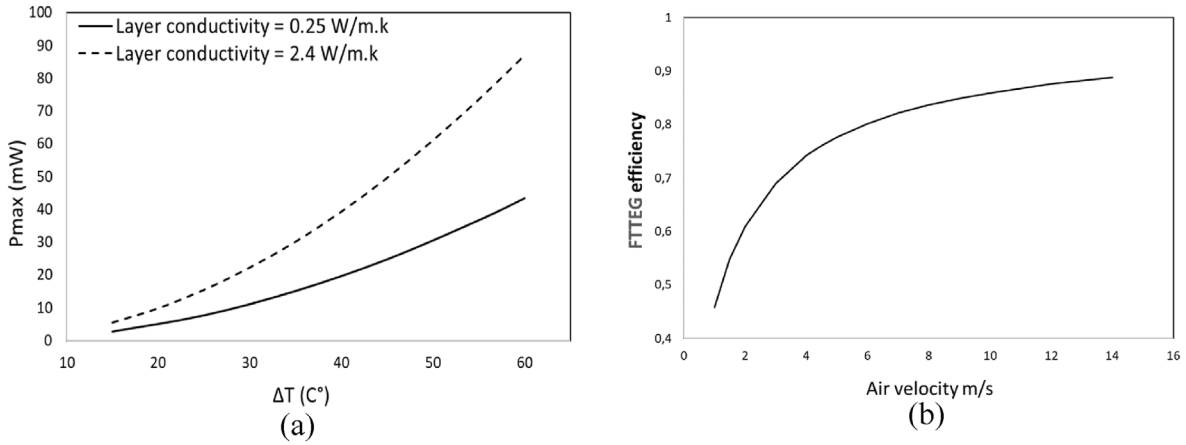

Fig. 10. (a) Influence of the resin layer conductivity on output power; (b) Dependency of the efficiency of a finned tube thermoelectric generator on cooling air velocity.

Table 4
Volume power density for tubular thermoelectric generators reported in the literature compared with that of the present work.

Reference	Materials	Nature	Elements Shape	ΔT (°C)	P_{max} (mW)	V_{active} (cm^3)	P_{max}/V_{active} (mW/cm^3)	$P_{max}/V_{active}/\Delta T$ ($mW/cm^3/°C$)
Min and Row [3]	Bismuth telluride	Bulk	Cylindrical	70	30	0.97	33.91	0.44
Jang et al. [7]	Skutterudite	Prouder	Cylindrical	425	13060	62.2	207.96	0.48
Merkulov et al. [33]	Cobalt-based oxide	Powder	Quadratic	430	138	0.58	239.58	0.56
Present work	Bismuth telluride	Bulk	Quadratic	60	16	0.46	34.56	0.58

power in the case of an isothermal fin assembly. A technoeconomic study would be required to optimize the energy consumed by the cooling system in a large-scale installation.

Given the high cost of inorganic thermoelectric materials, it is incumbent to consider the cost per watt of energy produced. To do this, the most appropriate indicator to use is the value of the volume power density. The volume power density is defined as the maximum output power of the TEG (P_{max}) divided by the volume of the active thermoelectric materials used in the device (V_{active}) [32]. A low volume power density implies lower economic feasibility.

Table 4 shows tubular thermoelectric generators reported in Refs. [3,7], and [33] compared with that developed in the present work. Due to the different temperature ranges of these investigations and to allow for a proper comparison, the volume power density was calculated by a temperature gradient of 1 °C and presented in the last column of Table 4. The results show a slightly better economic feasibility for the module used in the present work, which also has the smallest active volume and the lowest fabrication cost.

5. Conclusion

A novel finned tubular thermoelectric generator was designed, built, and characterized numerically and experimentally. The module combines quadratic-profiled bismuth/tellurium-based rigid thermoelectric elements and thin-disc cooling fins for waste heat recovery in gas/liquid applications. The goal is to develop a simple, robust, and compact design suitable for thermoelectric converters to harvest the energy released in industrial settings such as oil refineries. Resin was used in the assembly of the module to obtain a semi-rigid structure that is less likely to crack and could be cheaper to manufacture. Simulations and testing revealed encouraging results and parameters that affect module efficiency, such as contact resistance and resin layer effects. The output power of 16 mW and 600 mV in open-circuit voltage was generated in testing at a temperature gradient of 60 °C and a water temperature of 90 °C. It is concluded that conversion efficiency could be improved by taking into consideration the design and material quality parameters summarized below.

- Eliminating tube/fin thermal contact resistance by manufacturing the finned tube assembly as a single extruded piece.
- Selecting or developing a more thermally conductive and elastic resin.
- Adapting the fin and tube geometry to the physical and hydraulic properties of the thermal fluid used to recover waste heat.

Credit authorship contribution statement

Mohamed Amine Zoui: Conceptualization, Methodology, Software, Validation, Formal analysis, Investigation, Writing - Original Draft. **Said Bentouba:** Conceptualization, Methodology, Formal analysis, Writing - Review & Editing, Supervision, Project administration. **Nadjet Zioui:** Conceptualization, Writing - Review & Editing. **Dhayalan Velauthapillai:** Conceptualization, Writing - Review & Editing. **Mahmoud Bourouis:** Conceptualization, Methodology, Formal analysis, Writing - Review & Editing, Supervision, Project administration.

Declaration of competing interest

The authors declare that they have no known competing financial interests or personal relationships that could have appeared to influence the work reported in this paper.

Acknowledgements

The authors appreciate the technical assistance provided by Mr. J.G. Stockholm from Marvel Thermoelectrics (France) and for providing the thermoelectric materials used in the prototype.

References

[1] Zoui MA, Bentouba S, Bourouis M. The potential of solar thermoelectric generator STEG for implantation in the Adrar region. Algerian J Renew Energy Sustain Dev 2020;2:17–27. https://doi.org/10.46657/ajresd.2020.2.1.3.
[2] Zoui MA, Bentouba S, Stocholm JG, Bourouis M. A review on thermoelectric generators: progress and applications. Energies 2020;13:3606. https://doi.org/10.3390/en13143606.
[3] Min G, Rowe DM. Ring-structured thermoelectric module. Semicond Sci Technol 2007;22:880–3. https://doi.org/10.1088/0268-1242/22/8/009.
[4] Schmitz A, Stiewe C, Müller E. Preparation of ring-shaped thermoelectric legs from PbTe powders for tubular thermoelectric modules. J Electron Mater 2013;42:1702–6. https://doi.org/10.1007/s11664-012-2402-1.
[5] Takahashi K, Kanno T, Sakai A, Tamaki H, Kusada H, Yamada Y. Bifunctional thermoelectric tube made of tilted multilayer material as an alternative to standard heat exchangers. Sci Rep 2013;3:1501. https://doi.org/10.1038/srep01501.
[6] Sakai A, Kanno T, Takahashi K, Tamaki H, Yamada Y. Power generation and peltier refrigeration by a tubular π-type thermoelectric module. J Electron Mater 2015;44:4510–5. https://doi.org/10.1007/s11664-015-4017-9.
[7] Jang H, Kim JB, Stanley A, Lee S, Kim Y, Park SH, Oh M-W. Fabrication of Skutterudite-based tubular thermoelectric generator. Energies 2020;13:1106. https://doi.org/10.3390/en13051106.
[8] Shen Z-G, Wu S-Y, Xiao L. Theoretical analysis on the performance of annular thermoelectric couple. Energy Convers Manag 2015;89:244–50. https://doi.org/10.1016/j.enconman.2014.09.071.
[9] Zhang AB, Wang BL, Pang DD, Chen JB, Wang J, Du JK. Influence of leg geometry configuration and contact resistance on the performance of annular thermoelectric generators. Energy Convers Manag 2018;166:337–42. https://doi.org/10.1016/j.enconman.2018.04.042.
[10] Shen Z-G, Liu X, Chen S, Wu S-Y, Xiao L, Chen Z-X. Theoretical analysis on a segmented annular thermoelectric generator. Energy 2018;157:297–313. https://doi.org/10.1016/j.energy.2018.05.163.
[11] Fan S, Gao Y. Numerical analysis on the segmented annular thermoelectric generator for waste heat recovery. Energy 2019;183:35–47. https://doi.org/10.1016/j.energy.2019.06.103.
[12] Shittu S, Li G, Zhao X, Ma X, Akhlaghi YG, Ayodele E. High performance and thermal stress analysis of a segmented annular thermoelectric generator. Energy Convers Manag 2019;184:180–93. https://doi.org/10.1016/j.enconman.2019.01.064.
[13] Wen ZF, Sun Y, Zhang AB, Wang BL, Wang J, Du JK. Performance analysis of a segmented annular thermoelectric generator. J Electron Mater 2020;49:4830–42. https://doi.org/10.1007/s11664-020-08208-5.
[14] Mei Z, Morris JW. Characterization of eutectic Sn-Bi solder joints. JEM 1992;21:599–607. https://doi.org/10.1007/BF02655427.
[15] Bilirgen H, Dunbar S, Levy EK. Numerical modeling of finned heat exchangers. Appl Therm Eng 2013;61:278–88. https://doi.org/10.1016/j.applthermaleng.2013.08.002.
[16] Benmachiche AH, Tahrour F, Aissaoui F, Aksas M, Bougriou C. Comparison of thermal and hydraulic performances of eccentric and concentric annular-fins of heat exchanger tubes. Heat Mass Tran 2017;53:2461–71. https://doi.org/10.1007/s00231-017-2001-z.
[17] Chen H-T, Hsu W-L. Estimation of heat-transfer characteristics on a vertical annular circular fin of finned-tube heat exchangers in forced convection. Int J Heat Mass Tran 2008;51:1920–32. https://doi.org/10.1016/j.ijheatmasstransfer.2007.06.035.
[18] Mon MS. Numerical investigation of air-side heat transfer and pressure drop in circular finned-tube heat exchangers. PhD Thesis. 2003.
[19] Tahrour F. Modélisation et optimisation des échangeurs de chaleur à ailettes indépendantes. Sciences de La Matière; 2016.
[20] Ziolkowski P, Poinas P, Leszczynski J, Karpinski G, Müller E. Estimation of thermoelectric generator performance by finite element modeling. J Electron Mater 2010;39:1934–43. https://doi.org/10.1007/s11664-009-1048-0.
[21] Högblom O, Andersson R. Analysis of thermoelectric generator performance by use of simulations and experiments. J Electron Mater 2014;43:2247–54. https://doi.org/10.1007/s11664-014-3020-x.
[22] Tang D, Li D, Peng Y, Du Z. A new approach in evaluation of thermal contact conductance of tube–fin heat exchanger. Appl Therm Eng 2010;30:1991–6. https://doi.org/10.1016/j.applthermaleng.2010.05.001.
[23] Jeong J, Kim CN, Youn B. A study on the thermal contact conductance in fin–tube heat exchangers with 7mm tube. Int J Heat Mass Tran 2006;49:1547–55. https://doi.org/10.1016/j.ijheatmasstransfer.2005.10.042.
[24] Sheffield JW, Wood RA, Sauer HJ. Experimental investigation of thermal conductance of finned tube contacts. Exp Therm Fluid Sci 1989;2:107–21. https://doi.org/10.1016/0894-1777(89)90055-1.
[25] Savija I, Culham JR, Yovanovich MM, Marotta EE. Review of thermal conductance models for joints incorporating enhancement materials. J Thermophys Heat Tran 2003;17:43–52. https://doi.org/10.2514/2.6732.
[26] Liu Ju, Han Feng, Luo Xiaobing, Hu Run, Liu Sheng. A simple setup to test thermal contact resistance between interfaces of two contacted solid materials. In: 2010 11th international conference on electronic packaging technology & high density packaging. Xi'an, China: IEEE; 2010. p. 116–20. https://doi.org/10.1109/ICEPT.2010.5582472.
[27] Mirmira SR, Marotta EE, Fletcher LS. Thermal contact conductance of adhesives for microelectronic systems. J Thermophys Heat Tran 1997;11:141–5. https://doi.org/10.2514/2.6232.
[28] Fuqiang C, Yanji H, Chao Z. A physical model for thermoelectric generators with and without Thomson heat. J Energy Resour Technol 2014;136:11201. https://doi.org/10.1115/1.4026280.
[29] Ziolkowski P, Poinas P, Leszczynski J, Karpinski G, Müller E. Estimation of thermoelectric generator performance by finite element modeling. J Electron Mater 2010;39:1934–43. https://doi.org/10.1007/s11664-009-1048-0.
[30] Wei Z, Xie W, Ge B, Zhang Z, Yang W, Xia H, Wang B, Jin H, Gao N, Shi Z. Enhanced thermal conductivity of epoxy composites by constructing aluminum nitride honeycomb reinforcements. Compos Sci Technol 2020;199:108304. https://doi.org/10.1016/j.compscitech.2020.108304.
[31] Nayak SK, Mohanty S, Nayak SK. A new way synthesis of expanded graphite as a thermal filler to enhance the thermal conductivity of DGEBA resin as thermal interface material. High Perform Polym 2020;32:506–23. https://doi.org/10.1177/0954008319884616.
[32] Han M, Wee D. On the volume power density of radial thermoelectric generators. Int J Energy Res 2020;44:6049–57. https://doi.org/10.1002/er.5317.
[33] Merkulov OV, Politov BV, Chesnokov KYu, Markov AA, Leonidov IA, Patrakeev MV. Fabrication and testing of a tubular thermoelectric module based on oxide elements. J Electron Mater 2018;47:2808–16. https://doi.org/10.1007/s11664-018-6150-8.